Asthenospheric zircon below Galápagos dates plume activity

Yamirka Rojas-Agramonte (rojas@uni-mainz.de)
University of Mainz https://orcid.org/0000-0003-2019-6234

Boris Kaus
Institute of Geosciences & Computational Sciences Mainz, University of Mainz https://orcid.org/0000-0002-0247-8660

Andrea Piccolo
JGU, Universität Mainz

Ian Williams
ANU https://orcid.org/0000-0003-4465-6493

Axel Gerdes
Goethe-Universität

Jean Wong
The University of Hong Kong

HangXian Xie
Beijing SHRIMP Centre, Chinese Academy of Geological Sciences

Stephan Buhre
Johannes Gutenberg Universität

Theofilos Toulkeridis
Universidad de las Fuerzas Armadas ESPE

Pilar Montero
Universidad de Granada

Antonio Garcia-Casco
University of Granada https://orcid.org/0000-0002-8814-402X

Physical Sciences - Article

Keywords: mantle plumes, geodynamics, magma, tectonics

Posted Date: June 23rd, 2021

DOI: https://doi.org/10.21203/rs.3.rs-484102/v1

Asthenospheric zircon below Galápagos dates plume activity

Yamirka Rojas-Agramonte[1,2,3*], Boris J.P. Kaus[3], Andrea Piccolo[3], Ian S. Willians[4], Axel Gerdes[5,6], Jean Wong[7], HangXian Xie[2], Stephan Buhre[3], Theofilos Toulkeridis[8], Pilar Montero[9], Antonio Garcia-Casco[9,10*]

[1]Institut für Geowissenschaften, Christian-Albrechts-Universität zu Kiel, Ludewig-Meyn-Straße 10, 24118 Kiel, Germany

[2]Beijing SHRIMP Centre, Chinese Academy of Geological Sciences, 26 Baiwanzhuang Road, 100037 Beijing, China

[3]Institute of Geosciences, University of Mainz, 55099 Mainz, Germany

[4]Research School of Earth Sciences, Australian National University, Canberra, ACT 2601, Australia

[5]Department of Geosciences, Goethe-University Frankfurt, Altenhoferallee 1, 60438 Frankfurt am Main, Germany

[6]Frankfurt Isotope and Element Research Center (FIERCE) Goethe-University Frankfurt, Germany

[7]Department of Earth Sciences, The University of Hong Kong, Pokfulam Road, Hong Kong, China

[8]Universidad de las Fuerzas Armadas ESPE, Av. General Rumiñahui s/n y Ambato, Sangolquí – Ecuador

[9]Department of Mineralogy and Petrology, University of Granada, Fuentenueva s/n, 18071 Granada, Spain

[10]Andalusian Earth Sciences Institute (IACT), University of Granada-CSIC 18100 Armilla, Granada, Spain

*Corresponding authors: e-mail: rojas@uni-mainz.de; agcasco@ugr.es

Mantle plumes are active for long periods of time[1,2], however dating the onset of their activity is difficult. The magmatic products of the Galápagos plume, for example, have been subducted and fragmentarily accreted to the Caribbean and South American plates[3,4]. Based on submarine and terrestrial exposures it is inferred that the plume has been operating for ~90 Myrs[5] or perhaps even longer (e.g., ~139 Myrs[6]). Here we show that the activity of the plume dates back to ~170

Ma. Evidence for this comes from 0 to 168 Ma zircon with isotopic plume signature (Galápagos Plume Array; GPA) recovered from lavas and sediments from ten islands of the archipelago. Given lithospheric plate motion, this result implies that GPA zircon predating the Galápagos lithosphere (i.e., >14 Ma) formed at asthenospheric depths. Thermo-mechanical numerical experiments of plume-lithosphere interaction show that old zircon grains can be stored within local astenospheric stable domains to be later captured by subsequent rising plume magmas. These results open new avenues for research on mantle plume dynamics in similar tectonic settings.

Global tomography and numerical models suggest that mantle plume occurrences are closely linked to the margins of large low-shear velocity provinces (LLSVPs[7,8]). In these marginal zones, the ascent of material connects deep mantle dynamics with surface processes through mantle plume activity. This will eventually form large igneous provinces (LIPs), hotspot tracks and volcanoes[9], like the modern Galápagos Archipelago (Fig. 1), Hawai'i and Easter Islands. Recent studies suggest that despite striking differences in the surficial expression of the Galápagos, Eastern and Hawai'i plumes, they share a common generation mechanism originating at the Pacific LLSVP[10,11]. Mantle plume upwelling in the Pacific has been active since at least the mid-Jurassic, as recorded in the Pigafetta Basin, which contains the oldest oceanic crust of the Pacific plate (~170–160 Ma[12,13].

The Pacific plates exposed offshore Central America, Colombia-Ecuador, the Caribbean and associated accreted onshore rock exposures contain a Mesozoic to recent record of Pacific mantle upwelling events that resulted in new oceanic lithosphere, LIPs and hotspot tracks[14]. The early plume products range from early Cretaceous to the last Pacific LIP event: the Ecuadorian-Colombian-Caribbean LIP (ECCLIP) that formed mostly at ~90 Ma, with potential additional events in the range 139–74 Ma[2,5,6,15]. Though the ECCLIP is generally considered to be a product of the Galápagos plume, other authors however, based on paleomagnetic reconstructions, suggest that the ECCLIP originated 2000 km east of the Galápagos hotspot, and may thus not be derived from the same mantle plume[16].

The deep-rooted Galápagos mantle plume has generated several oceanic islands (<4 Ma old[17 and this study]) on top of a young oceanic lithosphere (10 Ma in the northern part of the Archipelago, 14 Ma in the southern part[18] created at the nearby Galápagos Spreading

Center (GSC; Fig. 1). Galápagos volcanoes are fed by a mix of plume- and asthenosphere-derived melts that provide important insight into heterogeneities of the mantle sources of ocean island volcanism[19]. Isotopic and trace element compositions of basaltic lavas in the Galápagos Archipelago indicate melting of several distinct mantle sources that include components from recycled oceanic and continental crust materials[20,21]. Palaeomagnetic and geochemical data record a complex interaction between the hot spot and the GSC[22]. The interplay between the mantle plume and the GSC dates back to Oligocene times (~23 Ma), when the Farallon plate tore into the Cocos and Nazca plates and the aseismic Cocos, Carnegie and Malpelo ridges formed[23,24]. Upon drifting away from the GSC, the oldest parts of these hotspot tracks have been subducted at the Central America and Nazca subduction zones (the oldest present-day ages of ridges are ~11–14 Ma[25,26].

We conducted an extensive sampling of basaltic and pumice rocks, inland deposits collected on the floor of a lava tube and, of sands from uphill stream beds and beaches (Figs. S1, S2, Fig. S3, Table S1) in 10 Galápagos islands (Figs. S1, S2; Table S1) covering most of the main area of the Archipelago. Thirty-seven (37) zircon-bearing samples were retrieved from the Central (Isabela 3 samples, Rábida 2, Santa Fe 5), Southern (Española 1, Floreana, 12), and Eastern (Baltra 2, Genovesa 1, Pinzón 2, San Cristobal 4, Santa Cruz 5) isotopic zones defined by[20]. From these samples we analysed 238 zircon grains for U-Pb dating and Hf and O isotopes compositions (see Supplementary Material for methods and description of the zircon grains). Many samples (including magmatic rock samples; Fig. 2a) contain a significant number of zircon crystals, most of which are <4 Ma old, indicating direct crystallization from magmas erupted in the islands. Twenty of these samples, however, contain zircon grains that significantly predate the spreading ridge- and plume-related magmatic evolution of the Archipelago and associated lithosphere (>14 Ma; Tables S2.1, S2.2).

The results of this study are displayed in Fig. 2 and show that, except for one grain (with a 21.0 Ma core and a 18.5 Ma rim; Fig. S4.1-2), all zircon grains with ages up to 168 Ma exhibit high positive $\varepsilon Hf_{(t)}$ (6–14; Tables S3.1, S3.2) and $\delta^{18}O_{(zircon)}$ values well within the range of mantle zircon[27] (4–6‰; Table S4). The zircon grains within this ~0–168 Ma range are distributed continuously without age gaps, defining a "Galápagos plume array" (GPA; Fig. 2a). Zircon younger than 0.2 Ma is rare (steep slope in Fig. 2b), given that most recent lavas are scarcely exposed to erosion. On the contrary, zircon in the range 0.2–4 Ma is the most abundant (shallow slope in Fig. 2b), indicating that lavas of that age

have the highest exposure to erosion in the different islands. GPA zircon that has pre-Galápagos ages in the range ~4–168 Ma is scarce (steep slope in Fig. 2b), but spreads evenly and is isotopically indistinguishable from the younger zircon, suggesting the same plume-related mantle origin.

The GPA trend is interrupted at 168 Ma (Fig. 2a) by the appearance of low $\varepsilon Hf_{(t)}$ and high $\delta^{18}O_{(zircon)}$ values in zircon of Triassic age (213 Ma) and older. The non-GPA zircon form a distinct array extending in ages from 213 to 3055 Ma with heterogenous $\varepsilon Hf_{(t)}$ and $\delta^{18}O_{(zircon)}$. Whereas zircon in the range ~213–835 Ma (plus the outlier zircon grain with a 21.0 Ma core and a 18.5 Ma rim) shows mostly low $\varepsilon Hf_{(t)}$ (-27.7–1.8, only two show higher values at 4.1 and 6.7) and generally high $\delta^{18}O_{(zircon)}$ (4.7–10.8‰), typical of continental crust, zircons in the range ~835–3055 Ma has a variety of $\varepsilon Hf_{(t)}$ (-9.1–8.2) and $\delta^{18}O_{(zircon)}$ (4.7–11.3‰) values consistent with both juvenile and continental crust signatures.

The non-GPA zircon grains indicate old (>213 Ma) to recent (~20 Ma, for the outlier) external sources not related to plume activity. The absence of continental basement below the Galápagos Archipelago[28,29] rules out the possibility of continental crust provenance, as could apply to other oceanic environments[30,31,32]. Given the uncertainty about the source of the exotic non-GPA zircons and because they are not direct magmatic products of plume activity, their provenance exceeds the scope of this study and is not further discussed here. Further discussions about transport mechanisms are nevertheless explored in the Supplementary Material.

The most ground-breaking finding of our extensive zircon study is the group of GPA zircons that pre-date the Galapagos lithosphere and with clear Hf and O isotopic mantle signatures. Given that the age of the Galápagos Islands lavas exposed to erosion is <4 Ma (Fig. 2b), that the Galápagos lithosphere is as young as 10–14 Ma[18] and plate motion has removed any older lithosphere from above the plume head, any juvenile GPA zircon older than 14 Ma must have formed in the asthenosphere and have been latter picked up by rising hot-spot magmas at asthenospheric depths (i.e., > ~50 km[28,33].

Two pre-Galápagos GPA zircon grains with ages of ~18 and 22 Ma are slightly younger than the time when the Farallon plate was split by the GSC (just above the plume head) and the Cocos and Carnegie ridges began to form (23 Ma[34]). This suggests that ridge-forming magmas did not fully escape from the plume head and crystallized zircon at

asthenospheric depths. The same reasoning can be extended to the other GPA zircon grains older than 23 Ma. During this time, a number of magmatic events took place, including the eruption of the Ecuadorian-Colombian-Caribbean LIP (ECCLIP) with a major phase of LIP construction at ~90 Ma[6]. Notably, we sampled two zircon grains (93 and 94 Ma) formed close to this major event (Fig. 2b). The GPA zircon also includes ages younger and older than the major ECCLIP event, clustering at early Tertiary (53, 55 and 65 Ma) and Jurassic (159, 164 and 168 Ma) times (Fig. 2b). The latter would allow expanding 30 Myrs back in time the magmatic history of the Galápagos plume recorded in its accreted dispersed fragments[6]. These GPA zircon data indicate that a) zircon is magmatic and juvenile, b) zircon formed much earlier than the recent lavas that brought them to the surface and formed the present-day Galápagos islands, and c) zircon formed in the asthenosphere and was stored at depth while staying unaffected by other plume-related magmatic events throughout the last ~170 Ma. These juvenile GPA zircon grains hence offer a unique opportunity to date the evolution of the mantle plume and to evaluate plume dynamics and asthenospheric flow.

A first-order observation is that our data places the onset of the Galápagos plume to at least ~170 Ma, much earlier than previously thought. We can, however, discard contamination. Even if most GPA zircon was sampled from surficial detritus, one of the oldest GPA zircon grains (i.e., 164 Ma), was sampled from a basaltic lava at the Alcedo Volcano on the uninhabited Isabela Island (Figs. 2b and S1). We can then rule out that this and other GPA zircons sampled from detrital material were delivered to the islands by surficial or anthropogenic processes. In addition, the presence of post- and pre-14 Ma GPA zircons in sands from almost virgin beaches and uphill streams (in the Baltra, Floreana, San Cristobal, Santa Cruz and Santa Fé islands) and inland lava tube deposits (Santa Cruz) clearly point to a local provenance from erosion of exposed volcanic rocks. Furthermore, a provenance study carried out on beaches from eleven islands of the archipelago shows that mineral grains and rock fragments derive from locally exposed basaltic rocks and excludes external sources[35]. All lines of evidence thus point to the crystallisation of 14–168 Ma GPA zircons in the sub-lithospheric source of Galápagos lavas.

Zircon forms after significant fractional crystallisation of primitive Zr-subsaturated basaltic magmas [e.g.,36,37] and is stable down to ~300 km depths, below which it transforms into reidite[38]. Experimental work shows that zircon can survive in the presence of mafic

melt for long periods of time as long as the volume of melt that interacts with a zircon crystal is small[39]. It is possible then that GPA zircon crystallised from near-solidus Zr-saturated evolved basaltic liquids at plume-head regions with limited melt fraction. Once formed, GPA zircon survived in hot mantle, even more so if the crystals are shielded within other mineral grains. If shielded within a Pb-free mineral (e.g., olivine), zircon grains can retain their U-Pb crystallisation ages even at 1500 ºC, independently of their residence time in the mantle[40]. Eventually, rapidly ascending magmas may pick up these zircon grains or zircon-bearing mineral or rock fragments. At this stage, dissolution of zircon occurred if not shielded and/or the magma resided long in a magma chamber. Ultimately, however, some asthenosheric zircon grains indeed survived and reached the surface in the crystallising magmas that, in turn, eventually reached Zr-saturation and formed new zircon, as demonstrated by many young zircon grains that date the onset of the present "IOB" Galapagos vulcanism at 4 Ma (Fig. 2b).

Our finding of old asthenospheric mantle zircon grains challenges current ideas about asthenosphere convection and plume/lithosphere interaction. Contrary to expectations from current understanding of asthenospheric motion, our finding implies that zircon was not dispersed by convective flow even after more than 100 Mys residence time in the asthenosphere. To explore whether this exceptional behaviour of the asthenosphere and associated processes are physically feasible, we carried out numerical thermo-mechanical simulations. Our reference scenario (Fig. 3) features a plume with a radius of 150 km and an excess temperature of 250 ºC with respect to the local mantle potential temperature, consistent with recent estimates from seismic tomography[41]. The plate has a constant velocity of 5 cm/yr, and an initial thermal age of 30 Ma (see Methods section for further details). After an initial rising stage, the plume head is sheared along with the moving plate, and splits into smaller plumes that produce partial melt beneath the lithosphere (Fig.3a). Zircons will form in these partially molten regions, which are coloured green or violet (depending on whether they consist of plume or ambient mantle material) to track their subsequent location. We initially introduce 90,000 passive tracers that represent zircon. The tracers are placed in the upper mantle and we track their motion once the mantle partially melts for the first time. Their subsequent path is tracked until they arrive in a partially molten region for the second time, when they are assumed to be extracted to the surface along with freshly erupting lavas. The zircon age is accordingly the age between formation and eruption (in Ma). Zircon that is transported to depths >300 km has

its U-Pb age reset upon reidite formation[e.g.,42] and is no longer considered in the interpretation.

The model results show that zircon can stay in the shallow upper mantle for extended periods of time (Fig. 3). Counterintuitively, not all zircon is dragged along with the moving lithosphere, but much instead initially moves in the opposite direction. This is because the plume's rising velocity is larger than the plate motion, which induces small scale convective cells (Fig. 3b-c). Some of this zircon returns to the plume area, whilst the rest is mixed in with the asthenospheric upper mantle. The dynamics of the plume is cyclic, with periods of slow and steady activity interrupted by more active phases. This results in discontinuous magmatic activity and sub-lithospheric circulation patterns that are mostly confined to the uppermost asthenospheric mantle, allowing the preservation of zircons. Most passive tracers are erupted to the surface within 50 million years of plume formation and contain young zircon (Fig. 3d and 3e). Yet, old zircons can be dragged into these lavas and erupt as well, in accordance with our observations in the Galápagos Archipelago.

In order to test the sensitivity of our results to changes in the model parameters, we performed over 20 simulations that demonstrate that the features described above are reproducible. The systematic analysis shows, however, that differences in the model results arise as a function of plume radius, temperature and oceanic plate age. Old oceanic plates (40 Ma) reduces the amount of melt produced, but can preserve very old zircons (~130 Ma), while young plates (15 Ma) generally give rise to a smaller amount of old zircons (see Fig. S5, S6 and Fig. S7). A smaller plume radius (<100 km) produces less melt, while higher plume temperatures result in a fully molten layer below the lithosphere with corresponding young zircon ages. Plate velocity and the manner in which a plume is introduced in the models are of second order importance.

Our results thus suggest that, once formed in a plume head, zircon crystals can remain within the asthenospheric mantle for extended periods of time. Following these results, the recorded asthenospheric zircon ages hence allow dating the Galápagos plume back to Jurassic times, a much older age than previously reported. Similar zircon observations and models of asthenospheric flow below ocean islands could apply to other plume-related hot spots. Therefore, a systematic analysis of zircon from ocean islands will allow monitoring temporal ranges of plume activity and dynamics over much longer periods

than those implied by the ages of the erupted lavas, hotspot tracks, plateaus and, eventually, plume-related terranes accreted to active continental margins.

References

1. Jellinek, A., Manga, M. The influence of a chemical boundary layer on the fixity, spacing and lifetime of mantle plumes. Nature 418, 760–763 (2002). https://doi.org/10.1038/nature00979.
2. Madrigal, P., Gazel, E., Flores, K. E., Bizimis, M. & Jicha, B. (2016). Record of massive upwellings from the Pacific large low shear velocity province. Nature Communications, 7(1), 1-12.
3. Gazel, E., Hoernle, K., Carr, M. J., Herzberg, C., Saginor, I., Van den Bogaard, P., Hauff, F., Feigenson, M., & Swisher, C. (2011). Plume–subduction interaction in southern Central America: Mantle upwelling and slab melting. Lithos, 121(1-4), 117-134.
4. Lynner, C., Koch, C., Beck, S. L., Meltzer, A., Soto-Cordero, L., Hoskins, M. C., Stachnik, J. C, Ruiz, M., Alvarado, A., Charvis, Ph., Font Y., Regnier, M., Agurto-Detzel, H., Rietbrock, A., & Porritt, R. W. (2020). Upper-plate structure in Ecuador coincident with the subduction of the Carnegie Ridge and the southern extent of large mega-thrust earthquakes. *Geophysical Journal International*, *220*(3), 1965-1977.
5. Sinton, C.W., Duncan, R.A., Storey, M., Lewis, J., Estrada, J.J., 1998. An oceanic flood basalt province at the core of the Caribbean plate. Earth Planet Sci. Let. 155, 222–235.
6. Hoernle, K., Hauff, F. van den Bogaard, P. (2004). 70 m.y. history (139-69 Ma) for the Caribbean large igneous province. Geology, 32, 697-700
7. Torsvik, T. H., van der Voo, R., Doubrovine, P. V., Burke, K., Steinberger, B., Ashwal, L. D., Trønnes, R. G., Webb, S. J. & Bull, A. L. (2014). Deep mantle structure as a reference frame for movements in and on the Earth. Proceedings of the National Academy of Sciences, 111(24), 8735-8740.
8. Garnero, E. J., McNamara, A. K., & Shim, S. H. (2016). Continent-sized anomalous zones with low seismic velocity at the base of Earth's mantle. Nature Geoscience, 9(7), 481-489.
9. Steinberger, B., & Torsvik, T. H. (2012). A geodynamic model of plumes from the margins of Large Low Shear Velocity Provinces. Geochemistry, Geophysics, Geosystems, 13(1).

10. Harpp, K. S., & Weis, D. (2020). Insights into the Origins and Compositions of Mantle Plumes: A Comparison of Galápagos and Hawai'i. Geochemistry, Geophysics, Geosystems, 21(9), e2019GC008887.
11. Harpp, K. S., Hall, P. S., & Jackson, M. G. (2014). Galápagos and Easter: A tale of two hotspots. Galapagos A Nat Lab Earth Sci, 204, 27-40.
12. Fisk, M., & Kelley, K. A. (2002). Probing the Pacific's oldest MORB glass: Mantle chemistry and melting conditions during the birth of the Pacific Plate. Earth and Planetary Science Letters, 202(3-4), 741-752.
13. Seton, M., Müller, R. D., Zahirovic, S., Williams, S., Wright, N. M., Cannon, J., Joanne M. Whittaker, Kara J. Matthews, Rebecca McGirr (2020). A global data set of present-day oceanic crustal age and seafloor spreading parameters. Geochemistry, Geophysics, Geosystems, 21, e2020GC009214. https://doi.org/10.1029/2020GC009214
14. Andjić, G., Baumgartner, P. O., Baumgartner-Mora, Cl. (2019). Collision of the Caribbean Large Igneous Province with the Americas: Earliest evidence from the forearc of Costa Rica. GSA Bulletin; 131 (9-10): 1555–1580. doi: https://doi.org/10.1130/B35037.1
15. Dürkefälden, A., Hoernle, K., Hauff, F., Wartho, J. A., van den Bogaard, P., & Werner, R. (2019). Age and geochemistry of the Beata Ridge: Primary formation during the main phase (~ 89 Ma) of the Caribbean Large Igneous Province. Lithos, 328, 69-87.
16. Boschman, L. M., van Hinsbergen, D. J., Torsvik, T. H., Spakman, W., & Pindell, J. L. (2014). Kinematic reconstruction of the Caribbean region since the Early Jurassic. Earth-Science Reviews, 138, 102-136.
17. Geist, D. J., Snell, H., Snell, H., Goddard, C., & Kurz, M. D. (2014). A paleogeographic model of the Galápagos Islands and biogeographical and evolutionary implications. The Galápagos: a natural laboratory for the earth sciences, 145-166.
18. Harpp, K. S., & Geist, D. J. (2018). The evolution of Galápagos Volcanoes: an alternative perspective. Frontiers in Earth Science, 6, 50.
19. Gazel, E., Trela, J., Bizimis, M., Sobolev,A., Batanova, V., Class, C., & Jicha, B. (2018). Long-lived source heterogeneities in the Galapagos mantle plume. Geochemistry, Geo physics, Geosystems, 19, 2764-2779. https://doi.org/10.1029/2017GC007338

20. Hoernle, K., Werner, R., Morgan, J. P., Garbe-Schönberg, D., Bryce, J., & Mrazek, J. (2000). Existence of complex spatial zonation in the Galápagos plume. Geology, 28(5), 435-438.
21. Blichert-Toft, J., & White, W. M. (2001). Hf isotope geochemistry of the Galapagos Islands. Geochemistry, Geophysics, Geosystems, 2(9)
22. Detrick, R. S., Sinton, J. M., Ito, G., Canales, J. P., Behn, M., Blacic, T., Cushman, B., Dixon, J. E., Graham, D. W. & Mahoney, J. J. (2002). Correlated geophysical, geochemical, and volcanological manifestations of plume-ridge interaction along the Galápagos Spreading Center. Geochemistry, Geophysics, Geosystems, 3(10), 1-14.
23. Hey, R. N. (1977). Tectonic evolution of the Cocos-Nazca spreading center, Geol. Soc. Am. Bull., 88, 1414 – 1420.
24. Wilson, D. S., & Hey, R. N. (1995). History of rift propagation and magnetization intensity for the Cocos-Nazca spreading Center. Journal of Geophysical Research: Solid Earth, 100(B6), 10041-10056.
25. Christie, D. M., Duncan, R. A., McBirney, A. R., Richards, M. A., White, W. M., Harpp, K. S., & Fox, C. G. (1992). Drowned islands downstream from the Galapagos hotspot imply extended speciation times. Nature, 355(6357), 246-248.
26. Werner, R., Hoernle, K., van den Bogaard, P., Ranero, C., von Huene, R., & Korich, D. (1999). Drowned 14-my-old Galápagos archipelago off the coast of Costa Rica: implications for tectonic and evolutionary models. Geology, 27(6), 499-502.
27. Valley, J. W., Lackey, J. S., Cavosie, A. J., Clechenko, C. C., Spicuzza, M. J., Basei, M. A. S., Bindeman, I. N., Ferreira, V. P., Sial, A. N., King, E. M., Peck, W. H., Sinha, A. K. & Wei, C. S. (2005). 4.4 billion years of crustal maturation: oxygen isotope ratios of magmatic zircon. Contributions to Mineralogy and Petrology, 150(6), 561-580.
28. Villagómez, D. R., Toomey, D. R., Geist, D. J., Hooft, E. E., & Solomon, S. C. (2014). Mantle flow and multistage melting beneath the Galápagos hotspot revealed by seismic imaging. Nature Geoscience, 7(2), 151-156.
29. Rychert, C. A., Harmon, N., & Ebinger, C. (2014). Receiver function imaging of lithospheric structure and the onset of melting beneath the Galápagos Archipelago. Earth and Planetary Science Letters, 388, 156-165.
30. Torsvik, T. H., Amundsen, H. E., Trønnes, R. G., Doubrovine, P. V., Gaina, C., Kusznir, N. J., Steinberger, B., Crofu, F., Ashwal, L. D., Griffin, W. L., Werner, S. C.,

& Jamtveit, B. (2015). Continental crust beneath southeast Iceland. Proceedings of the National Academy of Sciences, 112(15), E1818-E1827.

31. Ashwal, L. D., Wiedenbeck, M., & Torsvik, T. H. (2017). Archaean zircons in Miocene oceanic hotspot rocks establish ancient continental crust beneath Mauritius. Nature Communications, 8(1), 1-9.
32. Bea, F., Bortnikov, N., Montero, P., Zinger, T., Sharkov, E., Silantyev, S., Skolotnev, S., Trukhalev, A. and Molina-Palma, J.F. (2020). Zircon xenocryst evidence for crustal recycling at the Mid-Atlantic Ridge. Lithos, 354, 105361.
33. Gibson, S. A., & Geist, D. (2010). Geochemical and geophysical estimates of lithospheric thickness variation beneath Galápagos. Earth and Planetary Science Letters, 300(3-4), 275-286.
34. Harpp, K. S., Wanless, V. D., Otto, R. H., Hoernle, K. A. J., & Werner, R. (2005). The Cocos and Carnegie aseismic ridges: A trace element record of long-term plume–spreading center interaction. *Journal of Petrology*, *46*(1), 109-133.
35. Seelos, K., Rojas-Agramonte, Y., Kröner, A., Toulkeridis, Th., Inderwies, G., Buelow, Y. (2021). Composition and provenance analysis of beach sands in isolated sedimentary systems—a field study of the Galápagos Archipelago. American Journal of Science. https://doi.org/10.2475/05.2021.04
36. Pujol-Solà, N., Proenza, J. A., Garcia-Casco, A., González-Jiménez, J. M., Román-Alpiste, M. J., Garrido, C. J., Melgarejo, J. C., Gervilla, F., & Llovet, X. (2020). Fe-Ti-Zr metasomatism in the oceanic mantle due to extreme differentiation of tholeiitic melts (Moa-Baracoa ophiolite, Cuba). *Lithos*, *358*, 105420.
37. Davies, J. H. F. L.; Marzoli, A.; Bertrand, H.; Youbi, N.; Ernesto, M.; Greber, N. D.; Ackerson, M.; Simpson, G.; Bouvier, A. -S.; Baumgartner, L.; Pettke, T.; Farina, F.; Ahrenstedt, H. V.; Schaltegger, U. (2021). Zircon petrochronology in large igneous provinces reveals upper crustal contamination processes: new U–Pb ages, Hf and O isotopes, and trace elements from the Central Atlantic magmatic province (CAMP). Contributions to mineralogy and petrology, 176(1), 1-24.
38. Akaogi, M., Saki H., and Hiroshi K. (2018). Thermodynamic properties of ZrSiO4 zircon and reidite and of cotunnite-type ZrO2 with application to high-pressure high-temperature phase relations in ZrSiO4. Physics of the Earth and Planetary Interiors 281 (2018): 1-7.

39. Cambeses, A., Chakraborty, S., Dohmen, R., Sessing, J., Montero, P., Bea, F. (2020). Lifetime of Zircons in Mafic Melts: The Role of Melt Transfer and Storage Modes in the Mantle and Crust. https://doi.org/10.46427/gold2020.311
40. Bea, F., Montero, P., & Palma, J. F. M. (2018). Experimental evidence for the preservation of U-Pb isotope ratios in mantle-recycled crustal zircon grains. Scientific reports, 8(1), 1-10.
41. Nolet, G., Hello, Y., Lee, S. van der, Bonnieux, S., Ruiz, M.C., Pazmino, N.A., Deschamps, A., Regnier, M.M., Font, Y., Chen, Y.J., Simons, F.J., 2019. Imaging the Galápagos mantle plume with an unconventional application of floating seismometers. Sci Rep 9, 1326. https://doi.org/10.1038/s41598-018-36835-w
42. Rasmussen, C., Stockli, D.F., Erickson, T.M., Schmiederd, M. (2020). Spatial U-Pb age distribution in shock-recrystallized zircon – A case study from the Rochechouart impact structure, France. Geochimica et Cosmochimica Acta 273, 313-330

Methods

To avoid potential contamination from mineral separation equipment, the sand and soil samples were panned to yield heavy mineral concentrates on Galápagos beaches[43,44]. The basalt samples were processed at Mainz University, where extreme care was taken to avoid mineral contamination. Approximately 1–5 kg of sample was crushed to ~ 250 µm grain size using a jaw crusher and a roller mill.

The heavy mineral fraction was obtained using the panning technique and a Frantz magnetic separator at Mainz University followed by final panning with alcohol in the Beijing SHRIMP Centre, China. Zircons for isotopic analysis were handpicked under a binocular microscope and mounted in epoxy resin. About 100 g of the homogenized rock material were pulverized in a tungsten carbide mill (Siebtechnik) for chemical and whole-rock isotopic analysis. Zircon was analysed in situ for U-Pb and O isotopes using the SHRIMP II at the Beijing SHRIMP Centre, Chinese Academy of Geological Sciences, and for Hf isotopes using the LA-MC-ICP-MS at Hong Kong and Frankfurt Universities (Supplementary Tables S2.1, S2.2, S3.1, S3.2 and S4). The analyses were guided by optical and cathodoluminescence (CL) images (Supplementary Figures S4.1, S4.2). Analytical procedures are presented in detail in the Supplementary Material.

Geodynamic modelling approach

The numerical experiments herein showed have been performed using LaMEM[45,46], a visco-elasto-plastic finite difference code. LaMEM solves the fundamental conservation equation of mass (1), momentum (2) and energy (3) assuming the rocks to be incompressible:

$$\frac{\partial v_i}{\partial x_i} = 0 \quad (1)$$

$$\frac{\partial \tau_{ij}}{\partial x_j} - \frac{\partial P}{\partial x_i} + \rho g = 0 \quad (2)$$

$$\rho C_p \frac{DT}{Dt} = \frac{\partial}{\partial x_i}\left(k \frac{\partial T}{x_i}\right) + H_a + H_s + H_r \quad (3)$$

Where v_i are the component of the velocities along x_i direction, τ_{ij} are the component of the deviatoric stress tensor, P is the pressure, g is the gravity acceleration and ρ is the density. DT/Dt is the substantial time derivative of the temperature, C_p is the heat capacity, k thermal conductivity, H_a, H_s and H_r are the adiabatic, shear and radiogenic heat sources.

The conservation equations are solved in a fixed Eulerian frame of reference, using a finite difference staggered grid scheme, while the advection is explicit with time and performed using lagrangian particles and a second order Runga Kutta scheme. The lagrangian particles carries all the historical information needed to solve the equations.

Numerical Design: The main goal of our simulations is to understand if plume-lithosphere interaction is able to generate chemical distinct mantle domains that preserves geochronological information for a sufficient long period of time (i.e. >80 Myrs). Furthermore, we want to assess if some of these chemical heterogeneities can be captured again by the mantle plume flux during later model stage. For simplification, we do not consider the effects of radiogenic, adiabatic, and shear heating and assuming only a thermal dependent density and viscous constitutive models. We employ lateral inflow-outflow boundaries condition to simulate the motion of the oceanic plate, as well as a plume inflow boundary condition. To identify the potential domains that undergoes to chemical refinement, we interpolate the volumetric melt fraction (ϕ) from a precomputed mantle petrological phase diagram and track them using passive tracers.

Density depends on temperature and volumetric melt fraction:

$$\rho_{solid} = \rho_0(1 - \alpha(\mathrm{T} - \mathrm{T_{ref}})) \quad (4)$$

$$\rho_{eff} = \rho_{solid}(1 - \phi) + \rho_{melt}\phi \quad (5)$$

Where ρ_{eff} is the effective density, ρ_{solid} is the solid density, ρ_{melt} is the melt density, α is the thermal expansion, and T is the actual temperature and T_{ref} is the reference state temperature. We assume that melt feedbacks on density and viscosity reach their maximum effects at ϕ=0.08 (see eq. 5) as we do not explicitly account for melt extraction processes. The mantle phase diagram has been computed using Perple_X[47] using the pyrolite composition from[48], and using the solution model of[49] – for further references see[46]. All the relevant properties of each of the compositional phase are listed in Supplementary Table S6.

We employ a purely viscous constitutive model in our numerical simulation, using both linear (diffusion-creep) and non-linear (dislocation-creep) relations. The viscosity of the material has a lower and upper cutoff and the effective viscosity is the harmonic average between diffusion and dislocation creep and the cut-offs:

$$\eta_{tot} = \frac{1}{\eta_{diff}} + \frac{1}{\eta_{disl}} + \frac{1}{\eta_{upper}} \quad (6)$$

Where η_{tot}, η_{diff}, η_{disl}, and η_{upper} are the total effective, diffusion creep, dislocation creep, and upper cut-off viscosities respectively, whereas the minimum cut-off is introduced by adding a minimum stress in parallel to the viscoelastoplastic stress rheology. Diffusion and dislocation creep are computed using the law described in[50]:

$$\eta_{diff} = \frac{1}{2} B_{diff} \exp(-\chi\phi) \exp(-\frac{E_{act} + PV_{act}}{RT}) \quad (7)$$

$$\eta_{disl} = \frac{1}{2} B_{disl}^{\frac{1}{n}} \dot{\varepsilon_{II}}^{\frac{1}{n}-1} \exp\left(-\frac{\chi\phi}{n}\right) \exp(-\frac{E_{act} + PV_{act}}{nRT}) \quad (8)$$

B_{diff} and B_{disl} are the pre-exponential factor of diffusion and dislocation creep respectively. α is the pre-exponential factor to simulate the melt viscous weakening, n is the stress exponent, ε_{II} is the second invariant of the strain rate tensor, E_{act} and V_{act} are the activation energy and volume respectively (see Supplementary Table S6).

Initial setup & Boundary condition: We perform 2D numerical experiments using a domain that extends 4000 km x 1000 km along *x* and *z* direction and with a grid resolution of 256 x 128 elements along *x* and *z* direction. This strategy allows to perform long-term experiments able to cover the time evolution recorded by the geochemical data here presented. Moreover, employing such large numerical domains prevents inflow boundary condition to interfere with the processes that we simulate. The mantle is initially isothermal (1350 °C) using the half-space cooling model to describe the initial lithospheric thermal structure. The uppermost portion of the compositional field is composed by a thin oceanic crust (10 km), and 90 km of lithospheric mantle, while the rest of the domain is filled with mantle phases (i.e. upper and lower mantle). The thickness of the lithospheric mantle is self-adjusting during the evolution of the simulation as a function of the 1200 °C isotherm position. A depth dependent post-spinel phase transition at 660 km is introduced to adjust the inflow velocity of the plume allowing it to have a smooth temperature profile (the density jump associated with this phase transition is $\Delta\rho$ = 300 kg/m^3 see Supplementary Table S6). The initial plume is located at the bottom of the numerical domain and in its centre. In most numerical experiments (Supplementary Table S7), we introduce a rectangular thermal perturbation at the bottom to simulate an initial plume conduit to trigger the upwelling as soon as the simulation starts, which has the same phases as the plume and an excess temperature of 250 °C. Its width is equal to the inflow diameter (i.e. 300 km) and covers almost all the lower mantle with its height. Since, the zircon that have been collected from Galápagos are older than the Nazca plate, we assume that the pacific plate retains its integrity for the whole duration of the simulation. The initial age of the plate, and the temperature of the inflow boundary condition is varied from 15 Myrs to 40 Myrs and the plate velocity is varied from 1-10 cm/yrs.

We employ a free slip boundary condition at the upper boundary with a constant surface temperature of 0 °C. Lateral boundaries are no-heat flux and free slip boundary condition except for a narrow inflow-outflow window. The inflow-outflow window extends from the top of the domain to a minimum depth of 100 km to a maximum of 350 km. In all numerical experiments the velocity between 0 to 100 km along *z*-direction is constant, and it directed from left to the right side of the numerical domain. Then in most of the numerical experiments we introduce a buffer inflow-outflow window in which the velocity is linearly decreased to 0 km (the relax distance is varied from 0 to 250 km). The

inflow plate has a constant thermal age that increases towards the right as a function of the plate velocity. The bottom boundary is permeable with no tangential velocity components (following[51]), and the temperature at the boundary is constant and equal to the ambient mantle temperature (1350 °C) with a gaussian thermal perturbation with a radius of 150 km and a ΔT = 250 °C. Within the plume inflow window (-150, 150 km along x direction), particles with plume phase are injected with a temperature equal to the one of the bottom boundary condition. Outside this inflow window the temperature of the material is assumed to be equal to the ambient mantle temperature and has the same phase of the normal mantle.

Mantle chemical heterogeneities: In order to track the mantle chemical heterogeneities, we use two strategies: first, we highlight areas of the mantle or plume that reaches ϕ=0.05 at least once (i.e. we change the visualization phase, see **Fig. 3**); second, we activate passive tracers ('passive tracers zircon' in **Fig. 3**) that are associated with a chemical heterogeneous mantle domain and start tracking their position, temperature, pressure and melt quantity. The initial position of the passive tracers is defined by a refined grid spanning from -1200 to 1200 km and from 100 to 200 km along *x* and *z* direction respectively. As soon as they are activated, we record the age of the melting event, assuming that this portion of mantle could bear geo-chronological information (see Fig. 3). These mantle domains have to be interpreted as potential portions of the mantle that can bear zircon. Once the passive tracers melt again (when ϕ>0.05), we assume that the rising melts will bring the zircons to the surface and remove them from the model domain ('pre-eruption zircons' in **Fig. 3**). When the passive tracer is erupted, we collect information about the zircon age, and the timing at which the eruption event occurs (see **Fig.3**). The age of the potential zircon generated during the partially melting of the mantle is measured in Ma, while the actual simulation time is expressed in Myrs (as for the initial thermal age of the lithosphere). The chemical heterogeneous mantle domains that are tracked give an estimation of the age of the event that may lead to the generation of zircon population, and represents an estimation of the maximum age retained by them.

Reference Methods

43. Sevastjanova, I., Clements, B., Hall, R., Belousova, E. A., Griffin, W. L., & Pearson, N. (2011). Granitic magmatism, basement ages, and provenance indicators in the

Malay Peninsula: insights from detrital zircon U–Pb and Hf-isotope data. *Gondwana Research*, *19*(4), 1024-1039.,

44. Rojas-Agramonte, Y., Williams, I.S., Arculus, R., Kröner, A., García-Casco, A., Lázaro, C., Buhre, S.,Wong, J., Geng, H., Echeverría, C.M., Jeffries, T., Xie, H., Mertz-Kraus, R. (2017). Ancient xenocrystic zircon in young volcanic rocks of the southern Lesser Antilles island arc. Lithos, 290, 228-252.
45. Kaus, B. J., Popov, A. A., Baumann, T., Pusok, A., Bauville, A., Fernandez, N., & Collignon, M. (2016, February). Forward and inverse modelling of lithospheric deformation on geological timescales. In Proceedings of NIC Symposium.
46. Piccolo, A., Kaus, B. J., White, R. W., Palin, R. M., & Reuber, G. S. (2020). Plume—Lid interactions during the Archean and implications for the generation of early continental terranes. Gondwana Research, 88, 150-168.
47. Connolly, J. A. D. (2009). The geodynamic equation of state: what and how. Geochemistry, Geophysics, Geosystems, 10(10).
48. McDonough, W. F., & Sun, S. S. (1995). The composition of the Earth. Chemical geology, 120(3-4), 223-253.
49. Jennings, E. S., & Holland, T. J. (2015). A simple thermodynamic model for melting of peridotite in the system NCFMASOCr. Journal of Petrology, 56(5), 869-892.
50. Hirth, G., & Kohlstedf, D. (2003). Rheology of the upper mantle and the mantle wedge: A view from the experimentalists. Geophysical Monograph-American Geophysical Union, 138, 83-106.
51. Ribe, N. M., and Christensen, U. R. (1994). Three-dimensional modeling of plume-lithosphere interaction, *J. Geophys. Res.*,99(B1), 669– 682, doi:10.1029/93JB02386.

Acknowledgements This paper is dedicated to the memory of Alfred Kröner who sadly passed away on 22 May 2019 and was an inspiration during the initial stages of this project. This study was supported by the Deutsche Forschungsgemeinschaft (DFG) grant RO4174/3-1 and RO4174/3-3 to YR-A and SB, MINECO CGL2015-65824 and MICINN PID2019-105625RB-C21 to AG-C. BK acknowledges funding from ERC Consolidator Grant MAGMA #771143. YR-A Acknowledges the Prometeo Project of the Secretariat for Higher Education, Science, Technology and Innovation of the Republic of Ecuador. This is FIERCE contribution No. XX. The authors acknowledge the inputs of Mariana Cosarinsky who greatly improved the clarity of the manuscript.

Author contributions Y.R-A and A.G-C developed the original idea for the study, Y.R-A, I.W. H.X, A.G, J.W, S.B, dated the samples, Y.R-A and P.M. performed the data reduction of young zircon grains, B.K and A.P performed the geodynamic simulations. All authors including Th.T contributed to discussions and writing of the manuscript.

Competing interests The authors declare no competing interests.

Supplementary information the online version contains supplementary material available at

Figure captions

Figure 1: Plate tectonic configuration | Plate-tectonic configuration of the Pacific and the Caribbean region and location of uplifted and accreted ECCLIP (Ecuadorian-Colombian-Caribbean-Large-Igneous-Province) fragments. See supplementary Figure S1 for sample locations containing zircon grains.

Figure 2: Isotopic composition ($\varepsilon Hf_{(t)}$ and $\delta^{18}O_{(zircon)}$) and age of Galápagos zircons | A) U-Pb age vs $\varepsilon Hf_{(t)}$ (blue) and $\delta^{18}O_{(zircon)}$ (red) of analysed zircons. Both high $\varepsilon Hf_{(t)}$ and low $\delta^{18}O_{(zircon)}$ define the Galápagos Plume Array (GPA, blue and red rectangles, respectively), which extends from 0 Ma to ca. 170 Ma (note significant scatter at >170 Ma). B) Age of analysed zircons sorted by age of spot. The distribution shows four sectors separated by slope breaks, including 1: age range of zircon of less abundant (most recent) volcanic rocks exposed to erosion (<0.2 Ma); 2: age range of zircon of most abundant volcanic rocks exposed to erosion (0.2-4 Ma); 3 and 4: age ranges of pre-Galápagos Islands zircon, comprising 3: zircons belonging to the Galápagos Plume Array that extend from 4 to 168 Ma well beyond the oldest age of the exposed lavas and the age of basement oceanic lithosphere (10-14 Ma), and 4: exotic zircons older than 168 Ma with scattered $\varepsilon Hf_{(t)}$ and $\delta^{18}O$, including continental crust signature. For reference, 23 Ma (estimated split of Farallon plate) and 90 Ma (major ECCLIP event) are indicated in B. In A and B, lighter coloured circles for $\varepsilon Hf_{(t)}$ and age data, respectively, correspond to zircon grains separated from rock samples.

Figure 3: Numerical models of plume-lithosphere interaction | Snapshots **a-c** show the dynamics of a plume (with 1600 °C) interacting with a 30 Myrs old oceanic lithosphere that moves with 5 cm/yr to the right. Partially molten regions (indicated by purple shaded areas produce chemically distinct mantle domains (green/violet). We

565 additionally highlight the chemical heterogeneous mantle domain that undergoes the
566 zircon-reidite phase transition. The pathway of zircons in the mantle is tracked by
567 passive tracer zircons (circles) which are coloured by age until a zircon arrives at a
568 partially molten region for the second time when they are assumed are removed from
569 the numerical domain (indicated by stars). Both the age (**d**) and amount (**e**) of erupted
570 passive tracer zircons are tracked throughout the simulation and show that old zircons
571 can be preserved in the shallow mantle for extended periods of time.

572

Figures

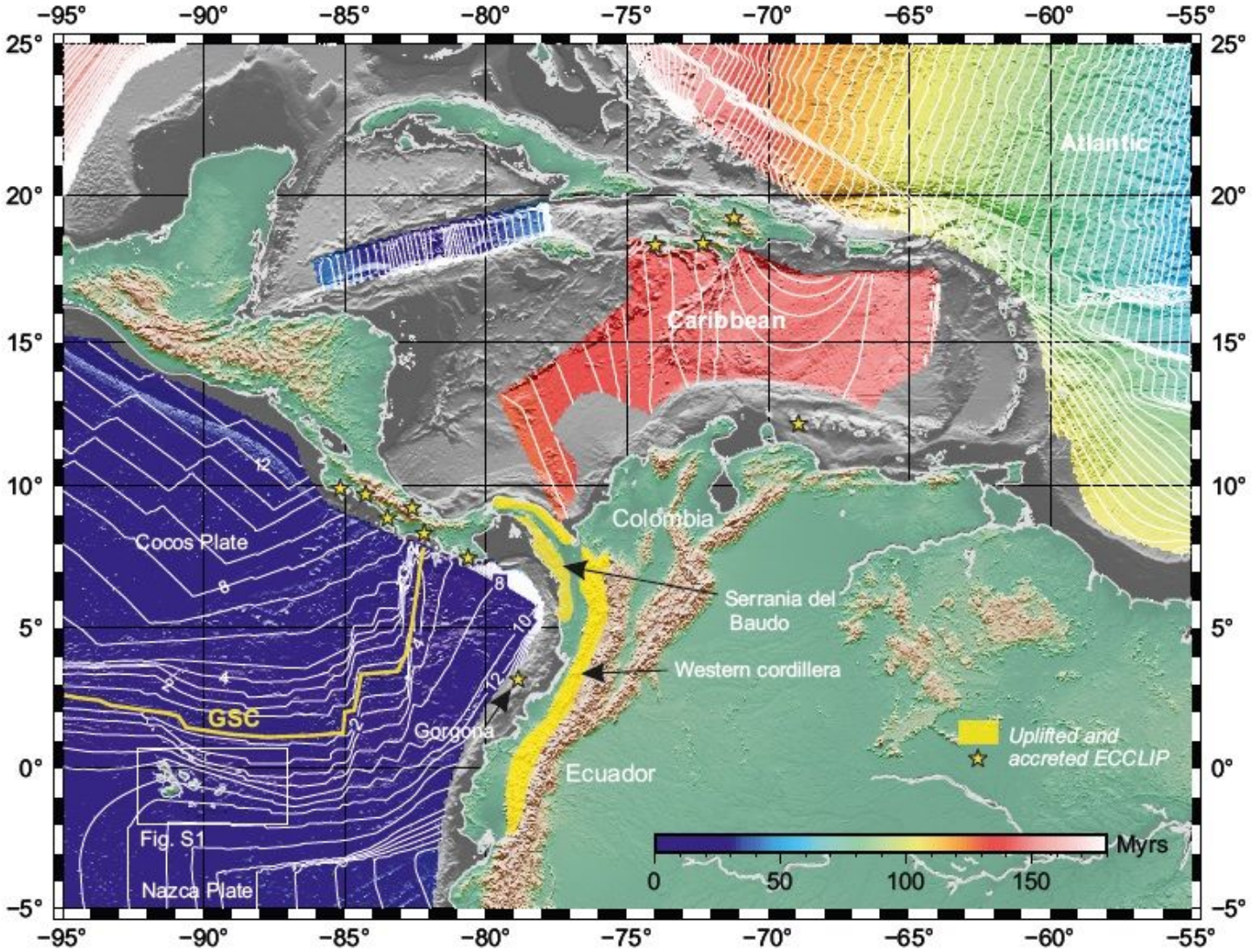

Figure 1

Plate tectonic configuration | Plate-tectonic configuration of the Pacific and the Caribbean region and location of uplifted and accreted ECCLIP (Ecuadorian- Colombian-Caribbean-Large-Igneous-Province) fragments. See supplementary Figure S1 for sample locations containing zircon grains.

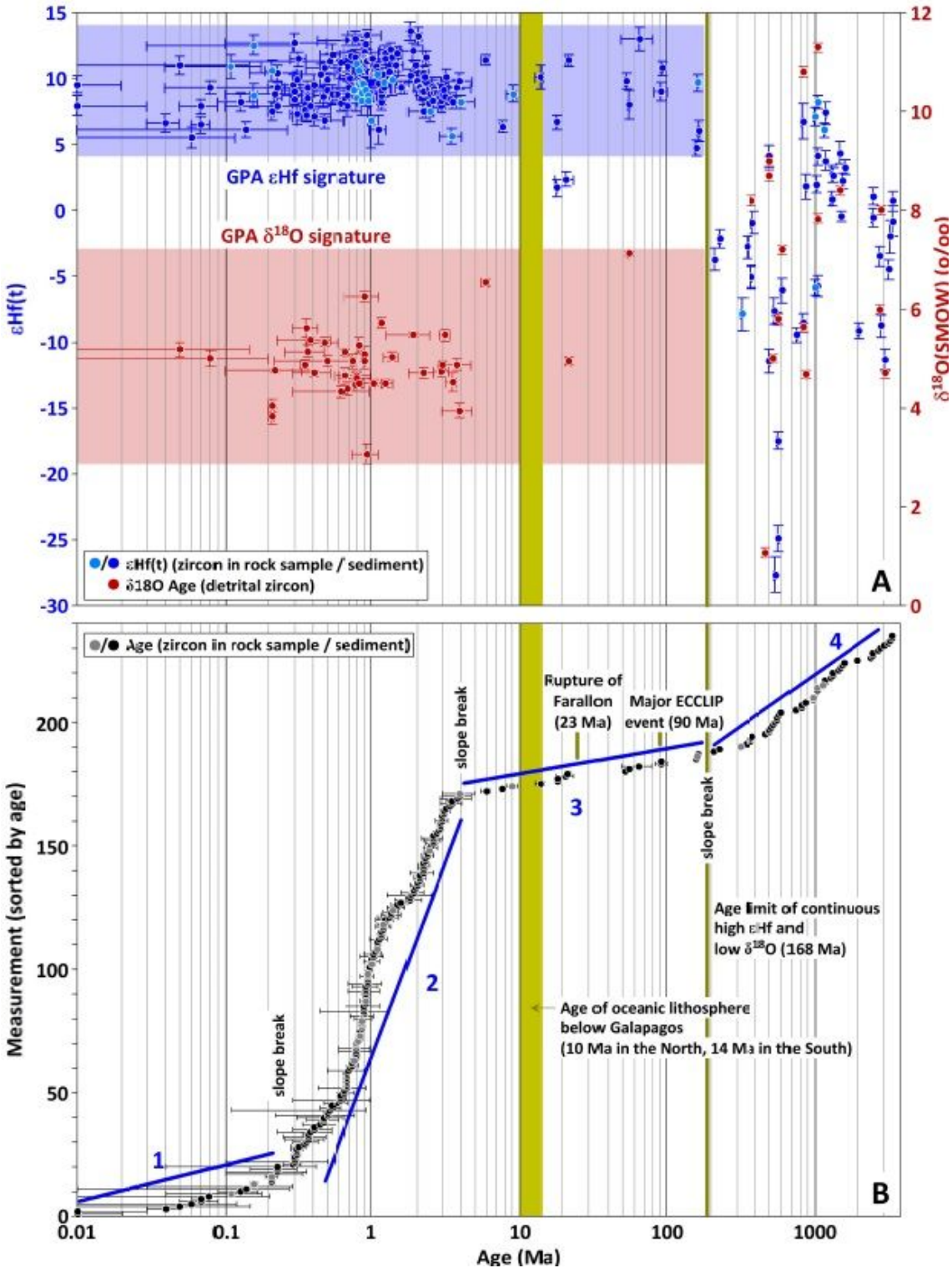

Figure 2

Isotopic composition (εHf(t) and δ18O(zircon)) and age of Galápagos zircons | A) U-Pb age vs εHf(t) (blue) and δ18O(zircon) (red) of analysed zircons. Both high εHf(t) and low δ18O(zircon) define the Galápagos Plume Array (GPA, blue and red rectangles, respectively), which extends from 0 Ma to ca. 170 Ma (note significant scatter at >170 Ma). B) Age of analysed zircons sorted by age of spot. The distribution shows four sectors separated by slope breaks, including 1: age range of zircon of less

abundant (most recent) volcanic rocks exposed to erosion (<0.2 Ma); 2: age range of zircon of most abundant volcanic rocks exposed to erosion (0.2-4 Ma); 3 and 4: age ranges of pre-Galápagos Islands zircon, comprising 3: zircons belonging to the Galápagos Plume Array that extend from 4 to 168 Ma well beyond the oldest age of the exposed lavas and the age of basement oceanic lithosphere (10-14 Ma), and 4: exotic zircons older than 168 Ma with scattered εHf(t) and δ18O, including continental crust signature. For reference, 23 Ma (estimated split of Farallon plate) and 90 Ma (major ECCLIP event) are indicated in B. In A and B, lighter coloured circles for εHf(t) and age data, respectively, correspond to zircon grains separated from rock samples.

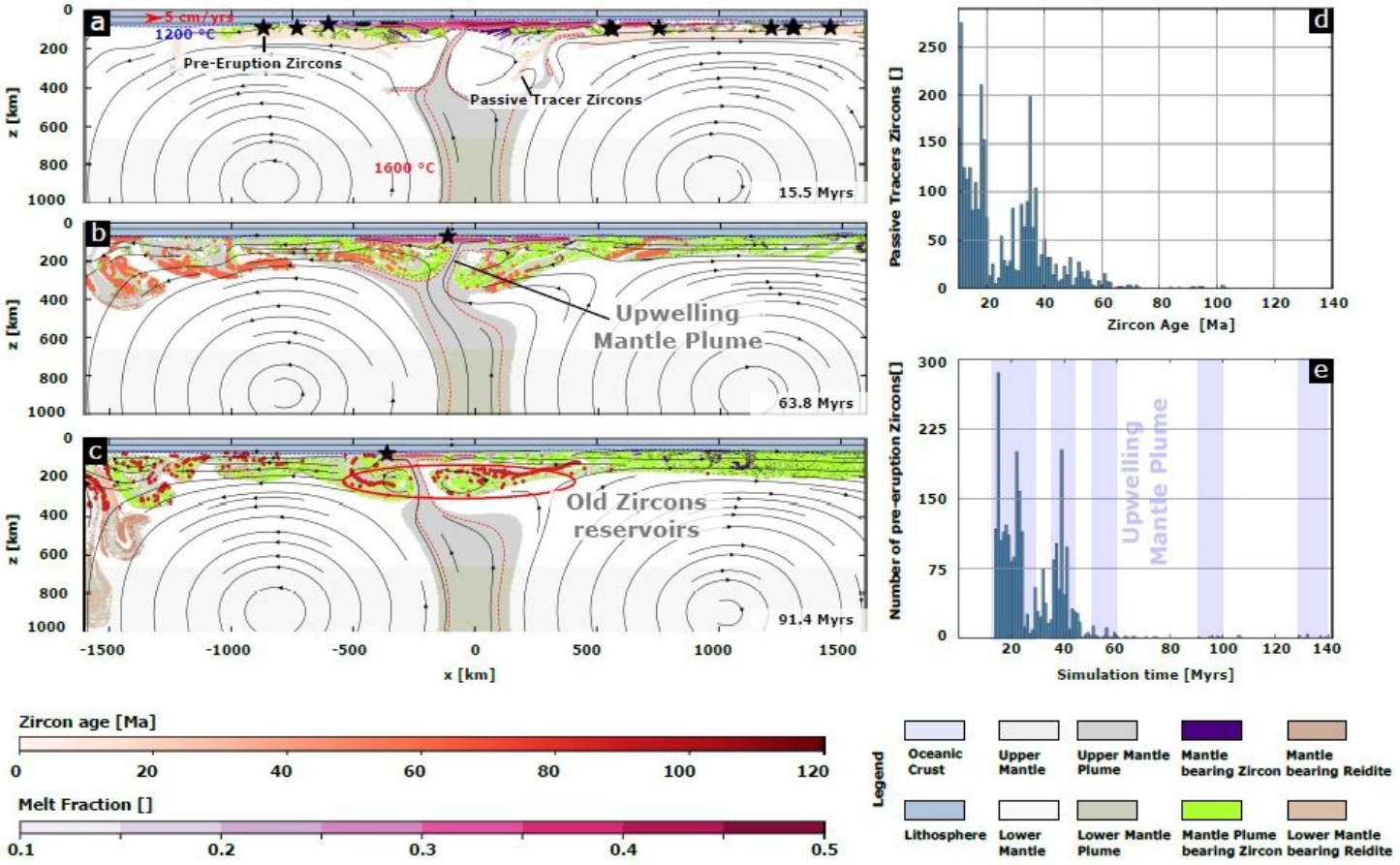

Figure 3

Numerical models of plume-lithosphere interaction | Snapshots a-c show the dynamics of a plume (with 1600 °C) interacting with a 30 Myrs old oceanic lithosphere that moves with 5 cm/yr to the right. Partially molten regions (indicated by purple shaded areas produce chemically distinct mantle domains (green/violet). We additionally highlight the chemical heterogeneous mantle domain that undergoes the zircon-reidite phase transition. The pathway of zircons in the mantle is tracked by passive tracer zircons (circles) which are coloured by age until a zircon arrives at a partially molten region for the second time when they are assumed are removed from the numerical domain (indicated by stars). Both the age (d) and amount (e) of erupted passive tracer zircons are tracked throughout the simulation and show that old zircons can be preserved in the shallow mantle for extended periods of time.

Supplementary Files

This is a list of supplementary files associated with this preprint. Click to download.

- SupplementaryTablesS1S5.xlsx
- SupplementaryTablesS6S7.docx
- FigureS1SupplementaryLocation.pdf
- FigureS2SupplementaryPhotos.pdf
- FigureS3SupplementaryGeoquimica.pdf
- FigureS4.1SupplementaryCLimages.pdf
- FigureS4.2SupplementaryCLimages.pdf
- FigureS5.pdf
- FigureS6.pdf
- FigureS7.pdf
- 12021SupplementaryInformation010521R.pdf